Proceedings of the 21st ICSMGE, Vienna, Austria, 14 – 19 June 2026. Pistrol, Adam & Schweiger (eds.)
Published by: ÖGG, Austrian Society for Geomechanics, Salzburg, Austria, ISBN 978-3-9503898-4-5
https://doi.org/10.53243/ICSMGE2026-455

Geophysical methods in tunnel look-ahead and deep soil mixing

Siau Chen Chian
Department of Civil and Environmental Engineering, National University of Singapore, Singapore, sc.chian@nus.edu.sg

Yun Zhou Tan
Cambridge Sensing, Science Park Drive, Singapore

Yanlong Niu
Earth Observatory of Singapore, Nanyang Technological University (formerly at National University of Singapore), Singapore

Yunyue Elita Li
Department of Earth, Atmospheric, and Planetary Sciences, Purdue University, United States of America

ABSTRACT: Fusion of geophysical methods in geotechnical engineering applications can offer complementary information on the mechanical properties of the ground. In this paper, geophysical methods involving seismic waves would be presented in two geotechnical engineering applications, namely, tunnel look-ahead and deep soil mixing. Tunnelling in complex geology and congested underground spaces in urban settings pose challenges for tunnel boring machines (TBMs) to operate efficiently and safely. Without the need for cutterhead access or through-lining drilling, geophysical seismic wave methods can travel and propagate through the ground to detect anomalies ahead of the TBM face. In the case of deep soil mixing (DSM), evaluating spatial mechanical properties of cement improved soil presents inherent challenges, primarily due to limited access below ground. Laboratory and field case studies would be presented on the use of quick and non-destructive seismic surface wave methods to estimate the development of unconfined compressive strength of cement stabilised soil over time, thereby offering enormous benefits of forecasting later-age strength of the improved ground, reducing the need for excessive coring of samples from the ground, as well as providing a three-dimensional evaluation of the extent of improved ground on site rather than spot measurements obtained from limited depth and location of the cored ground profile.

KEYWORDS: geophysical methods, tunnelling, ground improvement, surface wave.

1 INTRODUCTION

1.1 *Geophysical methods in geotechnical engineering*

Geophysical methods play a vital role in geotechnical engineering by providing valuable, non-intrusive insights into the subsurface conditions of a site. These methods can offer complementary information on the mechanical properties of the ground, thereby enhancing traditional site investigation techniques such as borehole drilling, standard penetration tests (SPT), and laboratory soil testing.

Techniques such as seismic refraction, electrical resistivity tomography (ERT), ground-penetrating radar (GPR), and multi-channel analysis of surface waves (MASW) allow engineers to estimate key parameters such as shear wave velocity, density, porosity, and subsurface layering. These properties are directly or indirectly related to the stiffness, strength, and deformation characteristics of soils and rocks, which are essential for assessing foundation performance, slope stability, and the overall suitability of a site for construction.

By integrating geophysical data with conventional geotechnical methods, engineers can improve the spatial coverage and reliability of subsurface models, reduce uncertainties in design parameters, and optimise the planning and safety of engineering projects. Moreover, geophysical techniques are often cost-effective and time-efficient, particularly across large or difficult-to-access areas, making them a valuable component of modern geotechnical investigations.

1.2 *Application in tunnelling*

Tunnel Boring Machines (TBMs) have transformed modern tunnelling by enabling simultaneous excavation and tunnel lining, significantly reducing surface disruption and improving safety, especially in densely populated urban areas. However, TBM operations remain vulnerable to unforeseen subsurface conditions. Geological anomalies such as underground voids, unexpected rock formations, and remnants of old infrastructure can lead to critical risks, including tunnel collapses, water ingress, and damage to the TBM cutterhead. Such events can result in substantial delays and financial losses amounting to millions of dollars (Klados, 1998; Tóth et al., 2013; Gong et al., 2016).

Current subsurface investigation methods, such as borehole drilling and surface-based geophysical surveys, provide essential data but are limited in spatial resolution and coverage. Boreholes offer only point-specific information (Marinos et al., 2008; Li et al., 2020), while surface geophysics can be impractical in constrained urban settings (Martí et al., 2008; Liu et al., 2017; Su et al., 2021). In-tunnel geophysical techniques, including Tunnel Seismic Prediction (TSP) and Horizontal Seismic Profiling (HSP), often require intrusive sensor deployment, making them less efficient and more expensive to implement.

To overcome these limitations, this study introduces SmartBoring, a novel high-resolution, in-tunnel seismic look-ahead technique. SmartBoring integrates geophysical theory (Li et al., 2017) with TBM-generated vibrations and controlled seismic sources to continuously acquire subsurface data without interrupting tunnel excavation.

Using principles of seismic wave propagation, SmartBoring reconstructs forward-looking seismic profiles to detect and interpret reflections from geological anomalies. This early-warning capability enables the identification of hazards before they impact TBM operations. Through numerical simulations and field case studies, this research demonstrates SmartBoring's potential to enhance geohazard prediction and risk mitigation, offering a safer and more efficient solution for tunnelling in complex urban environments.

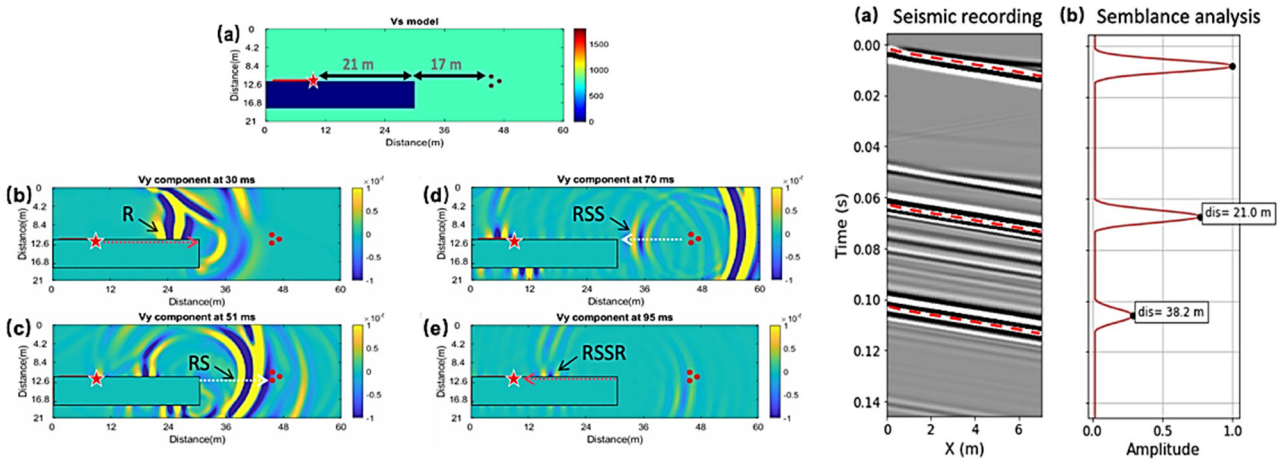

Figure 1. (Left) Simulated RSSR seismic wave propagation within the tunnel. (Right) (a) Seismic profiles recorded by the geophone array; (b) Corresponding semblance analysis.

1.3 *Application in deep soil mixing ground improvement*

Deep Soil Mixing (DSM), a widely used cement stabilisation method, enhances shear strength and reduces settlement in soft soils, making it vital for ground improvement projects (Kitazume & Terashi, 2013). Despite its advantages, DSM performance can be compromised by environmental factors and construction inconsistencies (Hino et al., 2012; Walske et al., 2016), highlighting the need for continuous and reliable monitoring during the curing phase to ensure quality assurance and cost control.

Non-destructive geophysical techniques, particularly seismic surface wave methods such as multichannel analysis of surface waves (MASW), provide an efficient and environmentally friendly alternative for subsurface characterisation. (Foti, 2003; Yao et al., 2019). However, traditional MASW applications often overlook the complex multi-mode responses and time-dependent effects introduced by high-stiffness cemented layers in DSM-treated soils (Niu et al., 2022), resulting in time-consuming manual mode identification and repeated inversion processes.

To overcome these challenges, this study proposes an advanced monitoring framework that integrates the generalised determinant misfit function with a Monte Carlo Tree Search (MCTS) algorithm. The misfit function addresses mode-numbering ambiguity in complex soil conditions (Maraschini et al., 2010; Zhang et al., 2022), while MCTS enables automated time-lapsed inversion by efficiently navigating the evolving search space using a tree-structured decision-making process (Świechowski et al., 2023).

Through synthetic tests and real-world DSM field experiments, the framework demonstrates its ability to track curing-induced changes in shear-wave velocity. The inverted Vs profiles are validated against conventional methods such as SPT, CPT and borehole sampling, confirming the framework's potential to deliver continuous, high-resolution, and operator-independent monitoring of mechanical property evolution in cement-stabilised soils.

2 SEISMIC WAVES IN TUNNEL LOOK-AHEAD

2.1 *Simulation*

The development of SmartBoring commenced with the application of three-dimensional finite-difference elastic simulations to examine seismic wave propagation in tunnel environments. These simulations allow for the observation of seismic signals generated behind the tunnel boring machine (TBM), which travel forwards, interact with subsurface anomalies, and reflect back to a geophone array mounted on the TBM.

As illustrated in Figure 1, the initial synthetic model assumed a homogeneous medium with a P-wave velocity of 1500 m/s and an S-wave velocity of 800 m/s. A group of concrete piles, each 0.9 m in diameter, was positioned 17 metres ahead of the cutterhead, while an active seismic source was located 21 metres behind it. A linear array of 24 geophones, spaced at 0.3 m intervals, was deployed to record the wavefield.

Rayleigh waves generated by the seismic source convert to S-waves upon reaching the cutterhead. These S-waves propagate forwards through the medium, reflect off subsurface obstacles, and reconvert into Rayleigh waves, which are then recorded by the geophones. This process illustrates the Rayleigh-S-wave-S-wave-Rayleigh (RSSR) propagation principle (Fang et al., 2024).

To analyse these recordings, a semblance method is employed to identify reflections from anomalies ahead of the tunnel face. This approach uses a normalised τ–p transform, which converts data from the time–offset domain into intercept time (τ) and slowness (p). Since both direct arrivals and reflected waves propagate at similar velocities within the tunnel, peak detection in the semblance curve is performed using the velocity of the first arrival.

To estimate the distance to potential anomalies, time-shift information from the reflected signals is extracted from the semblance results. The wave velocity used for this estimation is assumed to be approximately equal to the shear wave speed in the ground immediately behind the tunnel face—where the geophones are installed. By combining this estimated velocity with the measured time-shift, the distance to each obstacle is back-projected.

2.2 *Site setup*

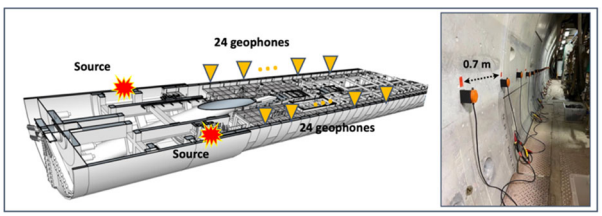

Figure 2. Schematic of the tunnel look-ahead system implemented in a field setting.

A total of 24 geophones were deployed along both sides of the tunnel, as shown in Figure 2. Seismic data were collected intermittently as excavation progressed, enabling continuous monitoring ahead of the TBM. This real-time detection system enhances operational safety and efficiency by allowing for early identification of geological anomalies.

2.3 *Case study*

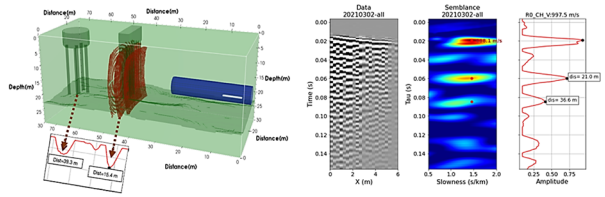

Figure 3. Schematic of tunnel alignment in Case Study I, showing two pile groups: Pile Group 1 located at Ring 52 (15.4 m from the TBM) and Pile Group 2 at Ring 98 (39.3 m from the TBM). The right-hand semblance panel illustrates the detection of Pile Group 1, with 21 m corresponding to the cutterhead location and 36.6 m to the pile anomaly.

This field trial was conducted as part of an underground Mass Rapid Transit (MRT) construction project in Singapore. The tunnel alignment intersected two known groups of abandoned piles. As shown in Figure 3, Pile Group 1 comprised three bored piles, each 900 mm in diameter, spaced between 1.2 m and 1.8 m. Pile Group 2 consisted of six micro piles with diameters of 350 mm and spacing ranging from 0.6 m to 1.5 m.

To validate the SmartBoring system's results, operational parameters from the TBM, such as torque, thrust force, and average penetration, were used to compute the penetration index, following the methodology proposed by Ergun et al. (2016). This approach supplements traditional borehole validation, which is often limited due to large spacing intervals (typically 25 m).

A strong correlation was observed between the seismic detection results, the mechanical behaviour of the TBM, and geological information as shown in Figure 4. This supports the viability of using TBM operational data as a validation tool. Despite potential variability due to cutter wear or operator influence, the integration of TBM parameters with seismic look-ahead data presents a promising strategy.

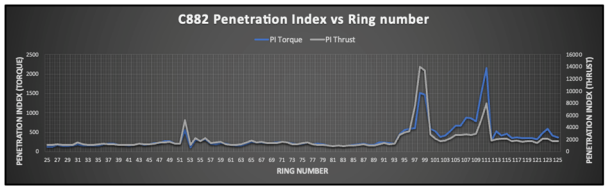

Figure 4. Penetration index related to the torque values. (blue) Penetration index related to the thrust force values.(grey) Three peaks are observed which correlate with the location of pile group 1 (R52), pile group 2 (R98) and rock/soil interface (R109).

2.4 *Accuracy analysis*

While SmartBoring is capable of detecting geological transitions ahead of the TBM, its accuracy may be affected by ambient noise and signal inconsistencies, potentially leading to false positives or missed anomalies. To address this, a Bayesian integration framework was developed to compile seismic signals from multiple acquisition points, allowing for uncertainty quantification and consistency assessment.

This approach capitalises on the overlapping detection ranges of successive measurements. By applying Bayesian inference, the system refines predictions by combining multiple independent observations into a statistically robust probability distribution (Figure 5). This method allows researchers to assign confidence levels to each anomaly detection and track uncertainty in real time.

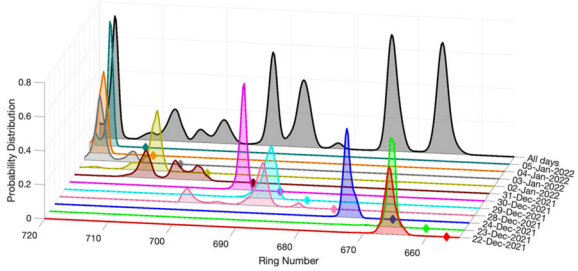

Figure 5. Bayesian updating using 11 continuous seismic tunnel look-ahead observations during TBM excavation through the Jurong Formation. Coloured curves represent individual observations; diamond markers show daily TBM cutterhead locations. The black curve indicates the posterior probability distribution after Bayesian integration.

3 SURFACE WAVES IN GROUND IMPROVEMENT

3.1 *Surface wave analysis framework*

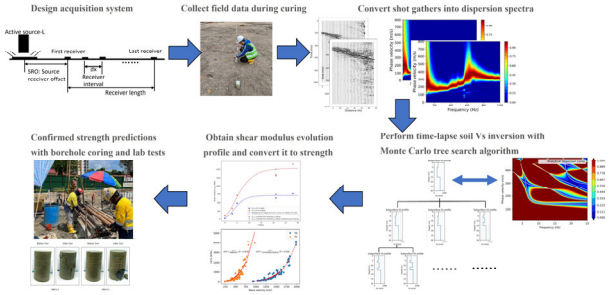

Figure 6. Workflow of evaluating the strength evolution for deep soil mixing.

This study presents a four-step framework for monitoring cement-stabilised soil properties using time-lapsed surface wave analysis: data acquisition, sequential inversion, property evaluation, and validation. As illustrated in Figure 6, the process begins with field acquisition during DSM curing, followed by dispersion spectrum extraction using the phase shift method. High-energy points in the frequency-phase velocity domain are identified as discrete data pairs for inversion.

The framework integrates these dispersion characteristics into a data-driven inversion process, combining a mode-independent forward operator with the Monte Carlo Tree Search algorithm. This approach addresses the challenges of multi-mode phenomena in complex subsurface conditions and eliminates the need for manual dispersion curve picking.

Time-lapsed Vs profiles are derived and used to compute shear modulus evolution in each DSM layer. The progression of small-strain stiffness is modelled using the Gompertz function to assess the effectiveness of cement stabilization over time.

Finally, the estimated shear modulus values are correlated with unconfined compressive strength through empirical relationships and validated against borehole coring results. This comprehensive, non-invasive approach ensures monitoring of DSM performance with strong potential for future industrial deployment.

3.2 *Site setup*

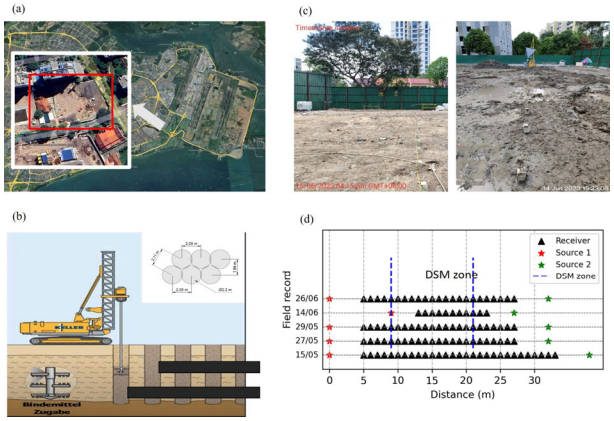

Figure 7. (a) Site location with a close-up aerial view of the DSM test area. (b) Schematic illustration of the DSM process and layout of cement columns. (c) Photographs of the field investigation before and after DSM treatment. (d) Surface wave monitoring record with the positions of the source and receiver, along with the acquisition timestamp.

A pilot surface wave monitoring experiment was conducted at a DSM site in the eastern part of Singapore, underlain by the heterogeneous Kallang Formation (Figure 7a). The site comprises soft silty sands and marine clays with extremely low shear strength (SPT-N values down to zero), necessitating deep soil mixing for ground improvement.

The DSM design layout is illustrated in Figure 7b, where overlapping cement columns with 2.2 m diameter and 2.05 m centre-to-centre spacing form two stabilised soil layers at depths of 7–11 m and 17–21 m, respectively. The design assumes lateral uniformity due to dense column overlap.

Figure 7c shows field photographs taken before and after DSM implementation, highlighting the surface conditions and site constraints during acquisition.

The surface wave monitoring setup is presented in Figure 7d. It employed 5 Hz 3C Smartsolo geophones with a 4000 Hz sampling rate, deployed across both treated and untreated zones. A sledgehammer striking a polyethylene plate served as the seismic source, with acquisition scheduled during equipment downtime to minimize noise. The array layout included a 5 m source-receiver offset and 1 m geophone spacing across a maximum spread of 29 m. Sensors were removed and repositioned after each session to maintain consistent levelling. Borehole samples collected on 14 June were tested for unconfined compressive strength and converted to shear modulus for validating surface wave–derived results.

3.3 *Case study*

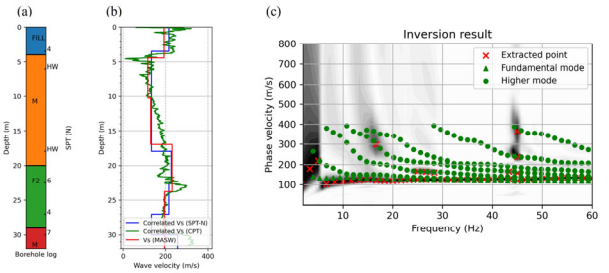

Figure 8. (a) Borehole log summary for the virgin ground; (b) Comparative subsurface Vs profiles derived from correlations using SPT-N, CPT, and MASW; (c) Dispersion spectrum for the virgin ground, with red 'x' markers showing the selected (f,V) pairs and green scatter points indicating inversion results, presented in a standard MASW format.

Figure 8 presents the MASW benchmark test conducted on virgin ground prior to DSM treatment. The borehole log (Figure 10a) confirms the presence of soft marine clay (7–19 m), classified as part of the Kallang Formation, with SPT-N values indicating extremely weak soil (labelled HM). Higher SPT-N values from 20–28 m suggest a transition to sandy clay within the Alluvial member, followed by deeper soft clay with organic content.

Figure 8b shows the inverted shear-wave velocity profile obtained using the proposed forward operator and Monte Carlo inversion. The result aligns well with Vs values derived from SPT and CPT correlations, validating the method's reliability. Figure 8c compares the observed dispersion spectrum with synthetic (f, V) pairs from the inversion, revealing a strong energy concentration at ~110 m/s above 10 Hz, consistent with soft surface layers. A velocity reversal pattern between 5–10 Hz indicates deeper low-velocity zones, characteristic of a complex subsurface structure.

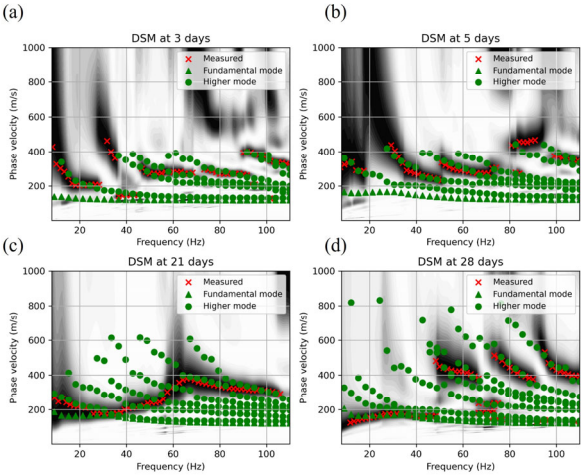

Figure 9. Field observations of the dispersion spectrum and inversion results in a conventional MASW view for different DS curing stages: (a) 3 days, (b) 5 days, (c) 21 days, and (d) 28 days post-curing.

Figure 9 presents the time-lapsed dispersion spectra and inversion results for two DSM layers, with six unknown parameters (depth, thickness, and Vs for each layer) estimated using the Monte Carlo Tree Search (MCTS) with 5,000 iterations. A fixed Vp/Vs ratio of 2.5 is assumed for cement-stabilized soils. Field tests were conducted on days 3, 5, 21, and 28 after DSM installation.

Figure 9a shows the observed dispersion spectrum on day 3, where higher mode energy becomes more prominent compared to virgin ground. Elevated phase velocities above 40 Hz indicate the presence of the first DSM layer, while a rise below 30 Hz corresponds to the second DSM layer. Energy concentration above 60 Hz is clearer than in untreated soil.

On day 5 (Figure 9b), phase velocities between 50–80 Hz increase, and higher mode energy becomes more dominant, reflecting early stiffness development in the treated zone. By day 21 (Figure 9c), further increases in phase velocity confirm ongoing curing, though limited receiver spread causes apparent dispersion artifacts.

Figure 9d illustrates significant energy intensification above 50 Hz with phase velocities exceeding 400 m/s, clearly separating fundamental and higher modes—consistent with Vs growth over time. However, frequencies below 30 Hz show reduced sensitivity to deeper layers, likely due to limited source energy penetration. Incorporating passive sources could improve low-frequency resolution for deeper DSM evaluation.

3.4 *Evaluation*

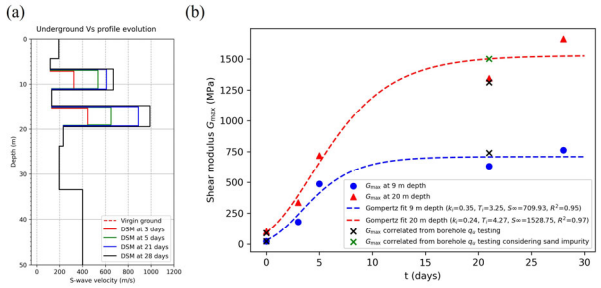

Figure 10. (a) Changes in subsurface Vs profiles during curing. (b) Time series of the inverted shear modulus at depths of 9 m (blue) and 20 m (red), with black 'x' symbols showing converted shear modulus values from borehole coring tests. Dashed red and blue lines represent Gompertz function fits.

Figure 10 illustrates the evolution of shear-wave velocity (Vs) and corresponding small-strain shear modulus (G_{max}) in two DSM-treated layers over the curing period, retrieved using the proposed inversion framework. As shown in Figure 10a, Vs increases significantly in both layers, confirming the effectiveness of cement stabilisation. The thickness and depth of the layers remain stable throughout, indicating negligible vertical movement of the cemented mass. The second DSM layer consistently exhibits higher Vs than the first, reflecting differences in the mechanical properties of the native soils, i.e. marine clay in the upper layer versus stiffer alluvial sand in the lower layer.

To assess the mechanical performance, Vs values are converted into G_{max} using cement-soil density. The G_{max} evolution is then modelled using the Gompertz function, which fits well with R^2 values of 0.95 and 0.97 for the first and second layers, respectively. Differences in model parameters reflect intrinsic contrasts in the stabilized soils. While both layers exhibit similar shear modulus growth rates, the second layer shows a delayed inflection time, suggesting reduced stabilisation efficiency due to its original soil composition.

Figure 10b compares G_{max} values derived from surface wave inversion with those converted from unconfined compressive strength (q_u) obtained via borehole coring at 21 days. Overall, the MASW-derived G_{max} aligns well with the laboratory-based estimates. However, a 12% underestimation is noted in the second layer, attributed to the influence of sand impurities in the soil, which are not accounted for in standard q_u-G_{max} correlations for clay.

Adopting from Chian et al. (2016), the q_u values are adjusted based on the liquid limit and water-cement ratio using a calibration equation from Niu et al. (2024). After correction, the G_{max} values (green crosses) align closely with the Gompertz model, confirming the reliability of the framework. Nonetheless, the results highlight the importance of site-specific soil characteristics in achieving accurate mechanical property assessments from geophysical data.

4 CONCLUSIONS

In the application of tunnelling, this research demonstrates the feasibility and practical value of a real-time, non-invasive tunnel look-ahead system using geophysical seismic wave principles for managing geological uncertainty. By combining seismic interferometry with probabilistic data fusion, SmartBoring offers a powerful tool for enhancing tunnel safety and performance, marking a significant advancement in underground construction technology.

To assess ground improvement using surface wave geophysical analysis, this research introduces a novel time-lapsed framework for monitoring the mechanical evolution of cement-stabilised soils. By integrating a mode-free forward operator with the Monte Carlo Tree Search algorithm, the framework enables automated Vs profile inversion with temporal constraints and minimal manual intervention. Synthetic and field data validate its accuracy and efficiency, capturing curing-induced Vs increases and complex multi-mode behaviour. The Gompertz model effectively quantifies shear modulus evolution, showing strong agreement with borehole results. This non-invasive, cost-effective approach holds promise as a standardised tool for evaluating DSM performance.

5 ACKNOWLEDGEMENTS

The tunnel look-ahead research was supported by the National Research Foundation, Singapore, and Ministry of National Development, Singapore under its Cities of Tomorrow R&D Programme (CoT Award COT-V3-2020-3).

The research on surface wave analysis in deep soil mixing technology was jointly supported by the Ministry of Education, Singapore, and Deltares, Netherlands.

Any opinions, findings, conclusions, or recommendations expressed in this material are those of the authors and do not reflect the views of the supporting organisations.

6 REFERENCES

Chian, S.C., Nguyen, S.T. & Phoon, K.K. 2016. Extended strength development model of cement-treated clay", Journal of Geotechnical and Geoenvironmental Engineering, ASCE, 142(2), 06015014.

Ergun, O.A., Erdoğan, C. & Ekinci, E. 2016. Analysis of the EPB-TBM excavation parameters used in a tunnel construction in Istanbul. In Proceedings of the 2nd World Congress on Mechanical, Chemical, and Material Engineering, Paper No. MMME 113.

Fang, G., Nilot, E.A., Li, Y.E., Tan, Y.Z. & Cheng, A., 2024. Quantifying tunnelling risks ahead of TBM using Bayesian inference on continuous seismic data. Tunnelling and Underground Space Technology, 147, 105702.

Foti, S. (2003). Small-strain stiffness and damping ratio of Pisa clay from surface wave tests. Géotechnique, 53(5), 455–461.

Gong, Q., Yin, L., Ma, H. & Zhao, J. 2016. TBM tunnelling under adverse geological conditions: an overview. Tunnelling and Underground Space Technology 57: 4–17.

Hino, T., Jia, R., Sueyoshi, S., & Harianto, T. (2012). Effect of environment change on the strength of cement/lime treated clays. Frontiers of Structural and Civil Engineering, 6(2), 153–165.

Kitazume, M., & Terashi, M. (2013). The deep mixing method. CRC press.

Klados, G. 1998. Experiences with hard rock shielded TBMs in special conditions, In Proceedings of 5th International Symposium on Tunnel Construction, 83–92.

Li, C., Hou, S., Liu, Y., Qin, P., Jin, F. & Yang, Q. 2020. Analysis on the crown convergence defor-mation of surrounding rock for double-shield TBM tunnel based on advance borehole monitor-ing and inversion analysis. Tunnelling and Underground Space Technology 103, 103513.

Li, S., Liu, B., Xu, X., Nie, L., Liu, Z., Song, J., Sun, H., Chen, L. & Fan, K. 2017. An overview of ahead geological prospecting in tunneling. Tunnelling and Underground Space Technology 63: 69–94.

Liu, B., Liu, Z., Li, S., Fan, K., Nie, L. & Zhang, X. 2017. An improved time-lapse resistivity tomog-raphy to monitor and estimate the impact on the groundwater system induced by tunnel excava-tion. Tunnelling and Underground Space Technology 66: 107–120.

Maraschini, M., Ernst, F., Foti, S., & Socco, L. V. (2010). A new misfit function for multimodal inversion of surface waves. GEOPHYSICS, 75(4), G31–G43.

Marinos, P., Novack, M., Benissi, M., Panteliadou, M., Papouli, D., Stoumpos, G., Marinos, V. & Korkaris, K. 2008. Ground information and selection of TBM for the Thessaloniki metro, Greece. Environmental & Engineering Geoscience 14: 17–30.

Martí, D., Carbonell, R., Flecha, I., Palomeras, I., Font-Capó, J., Vázquez-Suñé, E. & Pérez-Estaún, A. 2008. High-resolution seismic characterization in an urban area: Subway tunnel construction in Barcelona, Spain. Geophysics 73, B41–B50.

Niu, Y., Fang, G., Li, Y. E., Chian, S. C., & Nilot, E. (2024). Multi-Mode Rayleigh Wave Dispersion Spectrum Inversion Using Wasserstein Distance Coupled with Bayesian Optimization. GEOPHYSICS, 1–64.

Niu, Y., Li, Y. E., Chian, S. C., Nilot, E., & Fang, G. (2022). In-situ physical properties of reclaimed lands in Singapore. The Leading Edge, 41(5), 296–303.

Su, M., Liu, Y., Xue, Y., Cheng, K., Kong, F. & Guan, L. 2021. Detection method for boulders in subway shield zones based on data fusion multi-resistivity three-dimensional tomography. Bulletin of Engineering Geology and the Environment 80: 8171–8187.

Świechowski, M., Godlewski, K., Sawicki, B., & Mańdziuk, J. (2023). Monte Carlo Tree Search: A review of recent modifications and applications. Artificial Intelligence Review, 56(3), 2497–2562.

Tóth, Á., Gong, Q. & Zhao, J. 2013. Case studies of TBM tunneling performance in rock–soil interface mixed ground. Tunnelling and Underground Space Technology 38: 140–150.

Walske, M. L., McWilliam, H., Doherty, J., & Fourie, A. (2016). Influence of curing temperature and stress conditions on mechanical properties of cementing paste backfill. Canadian Geotechnical Journal, 53(1), 148–161.

Yao, K., Xiao, H., Chen, D.-H., & Liu, Y. (2019). A direct assessment for the stiffness development of artificially cemented clay. Géotechnique, 69(8), 741–747.

Zhang, D., Yang, B., Yang, Z., Zhang, M., Xiong, Z., Zhu, D., & Zhang, X. (2022). Multimodal inversion of Rayleigh wave dispersion curves based on a generalized misfit function. Journal of Applied Geophysics, 207, 104849.